Received: 7 August 2018 | Accepted: 21 December 2018

DOI: 10.1111/2041-210X.13144

RESEARCH ARTICLE

Methods in Ecology and Evolution BRITISH ECOLOGICAL SOCIETY

Leaf and wood classification framework for terrestrial LiDAR point clouds

Matheus B. Vicari[1] | Mathias Disney[1,2] | Phil Wilkes[1,2] | Andrew Burt[1] | Kim Calders[3] | William Woodgate[4]

[1]Department of Geography, University College London, London, UK

[2]NERC National Centre for Earth Observation, Leicester, UK

[3]CAVElab – Computational & Applied Vegetation Ecology, Ghent University, Gent, Belgium

[4]CSIRO Land and Water, Black Mountain, ACT, Australia

Correspondence
Matheus B. Vicari
Email: matheus.vicari.15@ucl.ac.uk

Funding information
CNPq (National Council of Technological and Scientific Development – Brazil), Grant/Award Number: 233849/2014-9; NERC NCEO; NERC Standard Grants, Grant/Award Number: NE/N00373X/1 and NE/P011780/1; CNRS Nouragues Travel Grants Program; ESA BIOMASS, Grant/Award Number: SR/02/355; European Union's Horizon 2020, Grant/Award Number: 640176; BELSPO (Belgian Science Policy Office), Grant/Award Number: SR/02/355

Handling Editor: Robert Freckleton

Abstract

1. Leaf and wood separation is a key step to allow a new range of estimates from Terrestrial LiDAR data, such as quantifying above-ground biomass, leaf and wood area and their 3D spatial distributions. We present a new method to separate leaf and wood from single tree point clouds automatically. Our approach combines unsupervised classification of geometric features and shortest path analysis.
2. The automated separation algorithm and its intermediate steps are presented and validated. Validation consisted of using a testing framework with synthetic point clouds, simulated using ray-tracing and 3D tree models and 10 field scanned tree point clouds. To evaluate results we calculated accuracy, kappa coefficient and *F*-score.
3. Validation using simulated data resulted in an overall accuracy of 0.83, ranging from 0.71 to 0.94. Per tree average accuracy from synthetic data ranged from 0.77 to 0.89. Field data results presented and overall average accuracy of 0.89. Analysis of each step showed accuracy ranging from 0.75 to 0.98. *F*-scores from both simulated and field data were similar, with scores from leaf usually higher than for wood.
4. Our separation method showed results similar to others in literature, albeit from a completely automated workflow. Analysis of each separation step suggests that the addition of path analysis improved the robustness of our algorithm. Accuracy can be improved with per tree parameter optimization. The library containing our separation script can be easily installed and applied to single tree point cloud. Average processing times are below 10 min for each tree.

KEYWORDS
3D point clouds, field data, LiDAR, material separation, simulated data, terrestrial LiDAR, testing framework

1 | INTRODUCTION

Terrestrial Laser Scanning (TLS) has seen a surge of new applications in forestry and ecology over recent years (Disney et al., 2018; Malhi et al., 2018). These include the accurate estimation of above-ground biomass (Calders et al., 2015; Gonzalez de Tanago et al., 2018; Momo Takoudjou et al., 2018; Raumonen et al., 2013), 3D vegetation density (Grau, Durrieu, Fournier, Gastellu-Etchegorry, & Yin, 2017), canopy profiles (Cuni-Sanchez et al., 2016), leaf area index and angle distribution (Zhao et al., 2015), tree structural parameters (Côté,

Fournier, Frazer, & Olaf Niemann, 2012; Côté, Widlowski, Fournier, & Verstraete, 2009) and even forest inventories (Liang et al., 2016).

Terrestrial laser scanners are active remote sensing instruments able to accurately generate a 3D point cloud of the surroundings by emitting laser pulses and reading their return signal. Distance is calculated by how long each pulse takes to travel from the scanner to a target and back (Jupp & Lovell, 2007). Using the distance information coupled with azimuth and zenith angles of emitted pulse, the scanner is able to generate 3D coordinates of each laser hit. Along with point coordinates, TLS scanners are able to measure the intensity of each return and some are even capable of recording the complete waveform of a set of pulses in multiple returns configuration.

Although many TLS ecological methodologies presented promising results, separating the mixture of materials in a point cloud, that is wood and leaf, remains one of the main challenges for the accuracy and reliability of these estimates (Ma et al., 2016; Woodgate et al., 2016; Zhu et al., 2018). In addition, if wood and leaf can be separated from single-wavelength LiDAR (which represents all current commercial TLS systems) it would open up many ecological applications for TLS data, particularly those to do with radiation transfer, gas exchange and net primary production partitioning of different materials. A robust separation method also offers the possibility of being applicable retrospectively to data collected in the past.

Côté et al. (2012) note that the presence of different materials makes a tree or forest point cloud extremely complex. Occlusion caused by the density of structures, such as different trees or even branches and leaves in the same tree, only increases the complexity of a TLS point cloud. Therefore, distinguishing between wood and leaf components is imperative to describe the tree structure accurately and to derive properties relating to the separate leaf or wood characteristics (Côté et al., 2012). According to Grau et al. (2017), when using indirect TLS methods, that is using the point cloud in a volumetric sense instead of pointwise information, the mixture of materials must also be considered. The authors state that preliminary classification of materials could help in correcting laser returns intensity in a volume by accounting for the proportions of each material present. The presence of woody material in the canopy, if not accounted for, can lead to overestimation in indirect methods to calculate leaf area index (Chen, 1996; Woodgate et al., 2016). This is supported by Hosoi, Nakai, and Omasa (2013), who stated that derivation of Leaf Area Density is affected by the separation of leaf and wood material in a point cloud.

Therefore, the successful separation of materials in a forest/tree point cloud has the potential to improve derivation of ecological variables from TLS point clouds. An additional challenge facing any attempt to separate wood and leaf is how to validate the results. True validation would require very detailed destructive sampling of scanned trees. As this is very rarely, if ever, possible or even desirable, published methods have relied on more qualitative or indirect comparisons. These include manual identification of wood and leaf points, purely visual inspection or comparisons with other indirect estimates, for example from gap fraction, or optical methods. Here, we propose a method to overcome this validation challenge using simulated point clouds, and 3D model simulations for which all properties are known/specified a priori.

1.1 | Current approaches to leaf-wood separation

Several approaches have been proposed to separate materials in a TLS point cloud. However, these methodologies are restricted in terms of their generality and/or rely heavily on user input. Such limitations hamper the potential of processing large number of trees. Separation methodologies in TLS data can be grouped based on their main approach: those using geometry (location and proximity of points), those using the intensity of returned points, or a mixture of both.

Béland, Widlowski, Fournier, Côté, and Verstraete (2011) and Béland, Baldocchi, Widlowski, Fournier, and Verstraete (2014) used the intensity of returns to separate leaf and wood points. This was an initial attempt to deal with the mixture of materials, albeit not as a dedicated method. Tao et al. (2015) presented a geometrical method to separate materials from a point cloud and compared it to a simple intensity threshold method. Their results indicated that the geometric method has a clear advantage. Also, the authors state that an intensity-based approach is, so far, not suitable for dense canopies as partial hits can generate misleading intensity values. Validation for this method used both simulated and field data. Although the use of simulated data is apparently promising, it is not clear how the authors obtained the reference classes to validate field data.

Another example of geometry-based separation is presented in Ma et al. (2016), which calculates a set of features for each point in the cloud and classifies them using Gaussian Mixture Models (GMM). This differs from Tao et al. (2015) as the local arrangement of points around each point is considered. As this method uses supervised classification, it can be trained to any tree structural archetypes and scan configurations. This approach is similarly applied in Zhu et al. (2018), albeit using a larger set of features and an adaptive neighbourhood search that aims to make this method more robust than that presented by Ma et al. (2016).

Using the intensity approach, Strahler et al. (2008), Douglas et al. (2012) and Danson et al. (2014), proposed new equipment configurations, with two lasers of different wavelengths (Douglas et al., 2015), that would greatly improve the ability to separate wood and leaf points (Danson, Sasse, & Schofield, 2018; Hancock, Gaulton, & Danson, 2017; Li, Schaefer, Strahler, Schaaf, & Jupp, 2018; Li, Strahler, et al., 2018). Different materials present different reflectance, and exploiting the contrast between wavebands would assist the identification of such materials. Although this idea could revolutionize how separation is performed, some technical issues prevent its adoption, such as the laser alignment. Another issue is that a dense canopy can increase the occurrence of mixed returns (Tao et al., 2015) and these can be confused with underlying spectral reflectance variations (Nevalainen et al., 2014). Also, the use of reflectance information requires more careful calibration of the LiDAR instruments, which is a challenge in itself (Calders et al., 2017).

It is also possible to use a combination of geometric and radiometric features, as presented in Zhu et al. (2018), which has the advantage

of increasing degrees of freedom in a classification without overfitting the data. Also, features calculated from different variables, for example point coordinates versus return intensity, may help to improve the separation robustness. When comparing results of current separation methodologies, geometry-based approaches obtained accuracies higher than those of intensity-based methods.

From results in the bibliography the use of geometric features yielded the best results. Ma et al. (2016) obtained overall accuracy for single trees of around 91%. Using similar approach, Zhu et al. (2018) obtained accuracies from 48% to 80% using only geometric features and, when combining geometric and radiometric features, overall accuracies improved to 80%–90%. Validations presented in these papers consisted primarily of visual inspection, that is manual identification of classified objects. Consequently, these results are hard to replicate and may contain bias. Furthermore, this reliance on manual assessment makes comparisons between methods and authors difficult.

Intensity-only approaches presented lower accuracies compared to geometric methods, with agreement coefficient (Cohen's κ) from 0.01 to 0.66 (accuracies from 18% to 78%) in Zhu et al. (2018) and κ of 0.71–73 in Tao et al. (2015). Table 1 shows a summary of separation methods found in the literature.

Even though new developments in multispectral equipment might improve intensity-based accuracies, the fact that this will not be applicable to existent data makes the case even further in favour of data-independent methods, such as geometric feature separation. Current geometry-based methods are dependent on user input to train classifiers (Ma et al., 2016; Zhu et al., 2018), which might slow down processing of large collections of trees. Also, validation of such methods relied upon comparison against visually identified classes and in some cases used data of a quality unlikely to be met in most practical applications, for example relatively small trees, isolated crowns and small presence of occlusion (Tao et al., 2015). Therefore, it is still unclear how such methods would perform in less-than-optimal conditions such as dense, tall tropical forests with significant understory and overlapping crowns. We take the geometric classification approach one step further using a mixture of approaches containing pointwise and path analysis classifications. Moreover, we present this in an automated framework developed to allow for simpler, faster prototyping of separation methods, while still ensuring robustness over different tree species, sensor configurations and data quality.

Here we present an open-source Python library that seeks to offer automated, easy to use and flexible separation from TLS point clouds. Our method builds on the approaches of Ma et al. (2016), with extra features from Wang et al. (2015), and extends their approach by including automated voting scheme and class selection, path classification and post-processing filters.

2 | MATERIALS AND METHODS

TLSeparation (Vicari, 2017b), was developed as an open-source Python library to perform leaf/wood classification from TLS data. The package includes classification, filtering and automated separation algorithms. It is designed be used as a flexible library to help develop custom separation workflows or, through already developed automated scripts, as a separation tool in its own right. Here we will present major components of this library and the validation performed to test an example of the automated separation script called *generic_tree*.

2.1 | Classification

The separation algorithm proposed here uses geometric features and structural analysis to classify individual tree point clouds into different materials. Four different algorithms are used, two based on pointwise geometric features and two based on so-called shortest path (SP) detection. Both pointwise algorithms are based on geometric features calculated in Ma et al. (2016) and Wang et al. (2015) but with improvements regarding classification and class labelling. As far are we are aware, our path detection algorithms, which consider the arrangement of points from a tree as a connected topological network, are an innovative approach to detect wood points. Using different classification methods ensures robustness over variations of tree structures and point cloud quality, making the approach as general as possible.

2.1.1 | Pointwise classification

Classification based on geometric features assume that different materials within the point cloud present different spatial arrangements, for example leaf points tend to be organized in small, planar

TABLE 1 Summary of methods proposed in literature for material separation from Terrestrial Laser Scanning tree data

Reference	Separation approach	Validation dataset	Validation method	Validation results
Tao et al. (2015)	G	1S; 2T	Visual and quantitative	Kappa coefficient from 0.79 to 0.89
Ma et al. (2016)	G	4F	Quantitative vs. manual classification	Overall accuracy of 95.45%
Zhu et al. (2018).	G, R, G+R	10F	Quantitative vs. manual classification	Geometric: 77.6%; Radiometric: 45.8%; Combination: 84.4%

Note. 'G' represents geometric features; 'R' represents radiometric features; 'S' represents simulated tree data; 'T' represents single tree data from field scans; and 'F' represents forest plot data from field scans.

clusters; wood/branch materials tend to be organized in more linear features. As eigenvalues can express data variability over orthogonally projected axes, they can be used as a base for quantitative metrics of the spatial arrangement of points.

Features are calculated here similar to Ma et al. (2016) but with additional features proposed by Wang et al. (2015). The geometry of each point is defined by calculating the eigenvalues of 3D coordinates using local subsets of points around it. The features listed in Table 2 are calculated using the normalized eigenvalues. Figure 1 shows an example of differences in geometric features for the same point cloud and indicates the potential for detecting different materials. These features are used to generate distribution models using GMM, which, when coupled with Expectation/Maximization (EM) algorithms, are classified into a predefined number of classes. Using EM in our classification means there is no need to perform manual training of the separation classes. This algorithm will randomly initiate a predefined number of GMMs, each one representing a class, and then start an iterative process that tries to find the set of parameters that maximize the log probability of the observed data (Do & Batzoglou, 2008). The EM will stop iterating when each point has been assigned to its most likely class.

Part of the separation process relies on accurately identifying each class. Here, two approaches are proposed to label the output from GMM classification as leaf or wood. The first selection compares the centre coordinates of each class in the feature space against absolute thresholds to determine which final class they belong to. These thresholds were selected for being in the boundary regions of GMMs representing different materials, which were generated from geometric features of a set of tree point clouds (see, e.g. for a single feature in Figure 4 below). The second approach calculates the distance between the centre coordinates of each class in the parameter space to the central coordinates of predefined reference classes. Each original GMM class, which can be predefined by the user, is then assigned the label of its closet reference class. The latter approach is similar to training the data using a default set of classes. However, a two-stage process, initially using an unbounded classification and then selecting classes, helps avoid bias in the classification.

Pointwise features are a direct function of neighbourhood sizes used. Using different neighbourhood sizes for the same point cloud can help capture changes in scale of tree structure, for example a large branch and a small branch would have similar geometric features in different scales. Therefore, a voting scheme is applied to the second pointwise classification (reference-based), allowing the use of different neighbourhood sizes in the same classification step. For each point, its most frequent class is selected as the final class.

TABLE 2 Geometric features used in the pointwise classification

Feature	Equation	Reference
1	λ_2	Ma et al. (2016)
2	$\lambda_0 - \lambda_1$	Ma et al. (2016)
3	$\lambda_1 - \lambda_2$	Ma et al. (2016)
4	$(\lambda_1 - \lambda_2)/\lambda_1$	Wang et al. (2015)
5	$\sum_{n=0}^{2} \lambda_i \times \log(\lambda_i)$	Wang et al. (2015)
6	$(\lambda_0 - \lambda_1)/\lambda_0$	Wang et al. (2015)

Note. Note that the λ_0 is the largest eigenvalue and λ_2 the smallest.

2.1.2 | Path detection

By assuming the tree is a network, in which each structure is connected to another leading from the base/root to the leaves, it is possible to apply a SP analysis to detect paths with high frequency of occurrence, for example trunk and larger branches (Figure 2a).

The detection starts with the conversion of the point cloud into a network graph, in which every point is represented by a node and connections between pairs of neighbouring points are represented by edges. Distance between points is used as edge weights. Once the graph is created, an SP analysis is performed from all nodes to the base node (lowest point in the point cloud). The path information is used in two approaches: retracing each node a given number of steps towards the base; and detecting nodes with high frequency of paths passing through.

Path retracing eliminates points on the extremities, where most of the leaf points tend to be located (Figure 2). A gap filling process is performed after the retracing. Local sets of remaining points are selected around each point detected by retracing. Points with a shorter path distance than the central (already detected) point of the local subset are masked as also detected. This process happens iteratively until no remaining points can be set as detected.

Path frequency detection assumes that nodes that are part of the trunk and larger branches will have a higher frequency of paths passing through them. A list containing all nodes that are part of each point's path to the base of the tree is created in the SP analysis. The number of times that each node is detected in these path lists is calculated and, because the frequency range escalates quickly with the number of points, the logarithm of path frequencies is used. Nodes with path frequency larger than half of the maximum log frequency are classified as wood. This threshold was chosen for generating results with overall highest accuracy over a range of trees tested, keeping the rate of false positives below 16% (i.e., leaf points classified as wood). Isolated nodes detected as wood are removed by checking the number of other nodes inside a fixed radius. For each node selected as wood, another fixed radius neighbourhood search is performed and all points inside this radius are also set as wood. Both these radii, 3 and 2 times the average distance between points in the cloud, were set to filter out points that are likely from leaf material and then to select neighbouring points that have a high probability of being also wood. The choices of radii were based on how the points for each material tends to be arranged close together.

Because of a fixed radius search across the whole point cloud, the frequency path detection is better suited to detect finer branching structures, whereas the retracing detection works better for stem and larger branches and thus both approaches are complementary (Figure 2b). Also, information about tree structure is robust to issues in point cloud quality, for example low density of points (Figure 3).

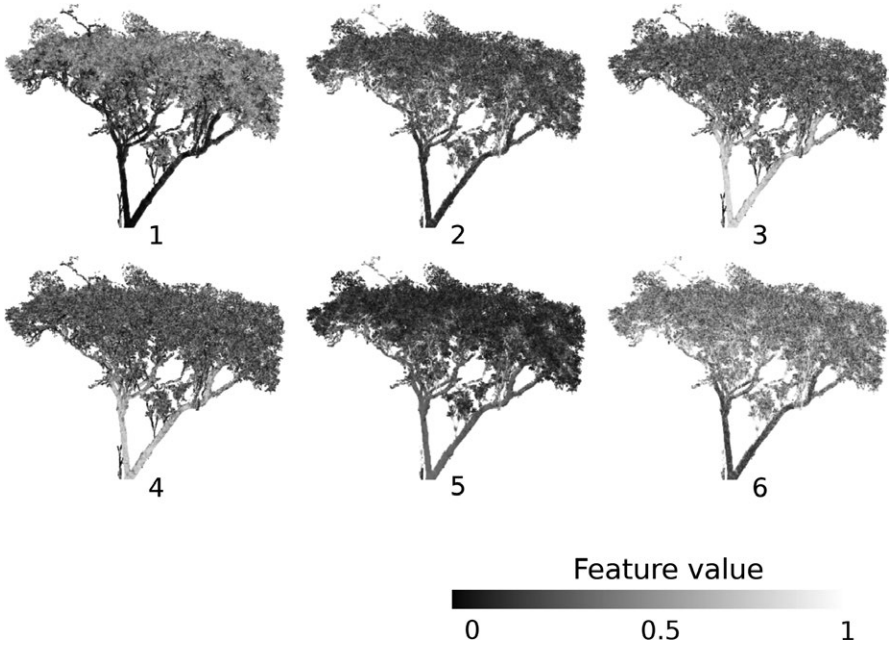

FIGURE 1 Example of geometric features calculated for a single tree (tree_2, height = 38.41 m; more details in section 'Field data' below). Numbers indicate index of geometric features as presented in Table 2. A fixed neighbourhood size of 50 points was used to calculate the features

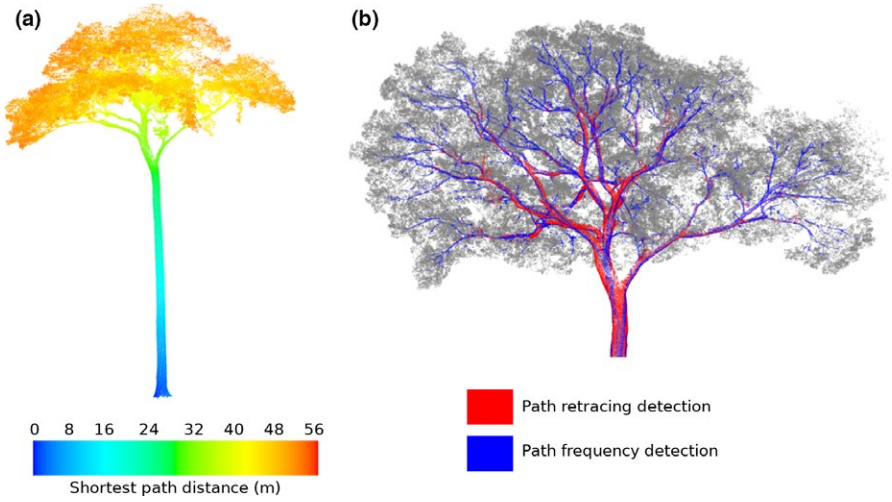

FIGURE 2 Example of shortest path (SP) distance (a) and SP detection results (b) for a graph generated from a tropical Terrestrial Laser Scanning point cloud (nouraguesH20_108 – details in 'Field data')

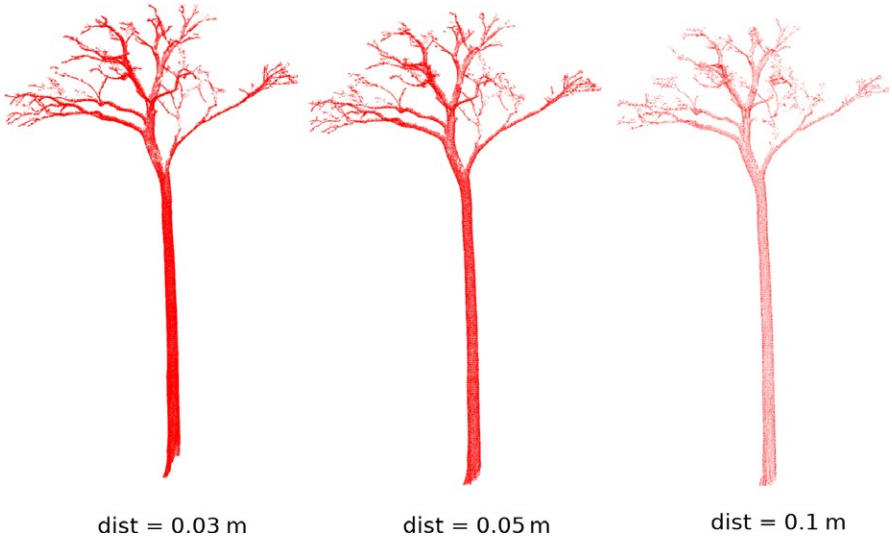

FIGURE 3 Example of wood points classified by retracing path detection from a single point cloud (nouraguesH20_108 – details in 'Field data') downsampled using three different distances

2.2 | Filtering

We developed four filters: majority filter, feature filter, cluster filter and path filter. These filters aim to improve separation accuracy especially on low-quality point clouds, with the presence of occlusion and noise in the upper portion of the canopy. The application of the filters is optional and modular, which means they can be applied in any combination desired in a separation workflow.

2.2.1 | Majority filter

Majority filter removes misclassified points by comparing each point against its neighbours' classes. The filter selects a subset of points around each point in the tree cloud and calculates class frequencies; each point is then assigned its most frequent surrounding class. Some options are available to fine tune this process, such as limiting which classes to change and the size of the neighbourhood.

2.2.2 | Feature filter

This filter is based on a simple threshold applied to the geometric feature 5 (Table 2). The same steps and neighbourhood parameters as in the pointwise classification are used, but it is only applied to points classified as wood. Points with feature value larger than −0.9 are kept. This threshold represents the boundary between elongated shapes and planar shapes in the features space and was selected by comparing values across points from different classes. Figure 4 shows multiple pairs of Gaussian models fitted to feature 5 for a number of tree point clouds (details in 'Field data').

2.2.3 | Cluster filter

The cluster filter uses DBSCAN (Ester, Kriegel, Sander, & Xu, 1996) to cluster a wood-classified point cloud. The only parameter for this filter is the maximum distance between points that are part of the same cluster. For our automated algorithm this distance was set as the mean distance of three closest neighbours from each point in the cloud. The ratios of three eigenvalues are calculated for each cluster using the same approach as in the geometric features. Clusters with ratio of first eigenvalue larger than 0.75 are kept. This means that only clusters with predominant projected dimension at least three times as large as the second and third projected dimensions, that is linear shape, are classified as wood.

2.2.4 | Path filter

Path filtering uses the same algorithm as in the retracing path detection but applied only on wood points, with a smaller number of steps to retrace. In this case, points in the extremities of a wood point cloud are set as leaf points.

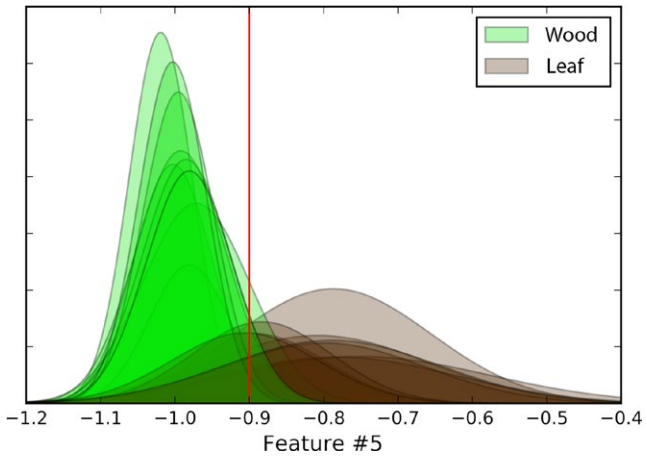

FIGURE 4 Example of multiple Gaussian models fitted to feature 5 calculated for a number of tree point clouds (more details in 'Field data'). Red line represents the selected feature threshold for *Feature filter*

2.3 | Automated separation algorithm

Figure 5 shows an overview of our separation script. This algorithm was validated with a combination of approaches using point clouds from four synthetic tree models and 10 scanned trees (see 'Validation'). Figure 5 shows how our classification algorithms are used in parallel, requiring four inputs: the tree point cloud to separate; a list containing one or more values for *k* nearest neighbours (default is [40, 50, 80, 100, 120]); the number of steps to retrace in the *Path retrace classification* (default is 40); and the voxel size used in both path classification steps (default is 0.05 m).

Filtering is applied after each classification step to avoid accumulating misclassified points. Because the spatial arrangement of wood points is consistent over different levels of point cloud quality (e.g. Figure 3), this separation workflow focuses on detecting as many wood points as possible and assumes that remaining points are from leaves. GMM classifications were performed twice, the first time applied on the entire point cloud, and then applied again to points initially classified as leaf. This second iteration aims to improve detection of linear structures, for example larger branches, that had features similar to initial leaf classes. A majority filter is included in each classification step. After results from the second GMM classification are filtered, they are merged with wood points from the first GMM and path detection steps. This is the approach we suggest to automatically separate single tree point clouds, which was selected because its combination of methods have shown to be the most robust among preliminary tests.

2.4 | Validation

Validation of the separation algorithm combined two sets of direct comparisons: using simulated point clouds, within the LiDAR Testing Framework LiDARtf (Vicari, 2017a), and manually classified randomly

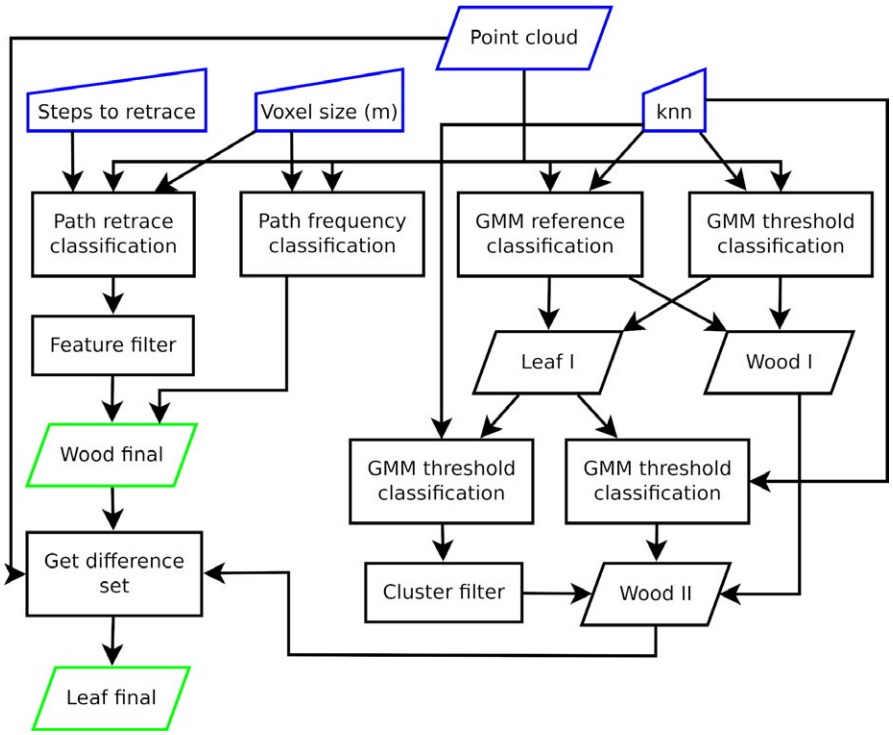

FIGURE 5 Example of main steps used in the automated separation algorithm *generic_tree* present in TLSeparation. GMM: Gaussian Mixture Model

sampled points from point clouds measured from real trees. Access of datasets used in the validation is presented in 'Data sources'.

The major advantage of using model trees and simulated point clouds in this way is that all components of the system, from end-to-end are known. As a result this is a true 'validation' of the resulting separation, albeit with the caveat that these are synthetic trees. Validation of separation methods on real TLS data will always be very limited except in (the very few if any) cases where comprehensive destructive sampling is carried out.

2.4.1 | Testing framework

LiDARtf was used to test the separation algorithm. Datasets were simulated from four 3D tree models used extensively to benchmark radiative transfer models as part of phase IV of the Radiative Transfer Model Intercomparison exercise (Widlowski et al., 2015), as show in Table 3. Foliage material in these models is defined by a single leaf replicated throughout the tree crowns. Leaf models have distinct shapes for each tree and different sizes (see Widlowski et al., 2015 for more details), which might impact the simulated scans capability of resolving finer leaf shapes.

A Monte-Carlo ray tracing library, *librat* (Disney, Lewis, & Saich, 2006; Lewis, 1999; Widlowski et al., 2015), was used to simulate 120 TLS 'scans' for each tree. Scans were simulated using configurations based on fieldwork campaigns (see e.g. Calders et al., 2015; Wilkes et al., 2017), with the scanner positioned 1.5 m from the ground and in a grid pattern around each tree, with spacing of 5 m between each scan location. Combinations of simulated clouds were merged to generate datasets. This process used pseudo-random sampling to select and merge between 1 and 10 unique clouds from the set of 120 simulations. In total 50 combinations were generated for each tree (e.g. available in the Supporting Information).

2.4.2 | Field data

A second validation was performed using real point clouds from 10 trees covering different species, locations and LiDAR scan settings (Table 4). Examples of these clouds are shown in the Supporting Information. A RIEGL VZ-400 was used for scanning all trees. This scanner has a wavelength of 1,550 nm, beam divergence of 0.35 mrad and measuring range of about 600 m (RIEGL Laser Measurement Systems GmbH). For each tree, 200 points were pseudo-randomly

TABLE 3 Characteristics of tree models used to validate our separation method (Widlowski et al., 2015)

Species	Identifier (RAMI-IV)	Height (m)	DBH (m)	Single leaf area (cm^2)
Acer platenoides	ACPL	15.37	0.115	139.6
Almus glutinosa	ALGL3	25.76	0.28	23.4
Betula pendula	BEPE2	25.49	0.175	20.7
Tilio cordata	TICO2	11.27	0.09	52.5

Note. RAMI-IV: phase IV of the Radiative Transfer Model Intercomparison.

TABLE 4 Validation data description

Point cloud	Scan location	Tree height (m)	Number of points	Angular resolution (°)	Scanning pattern
1	Alice Holt (UK)	19.58	474,712	0.06	Circle around the tree
2	Alice Holt (UK)	22.23	1,944,116	0.06	Circle around the tree
3	Alice Holt (UK)	19.9	802,004	0.06	Circle around the tree
4	Caxiuanã (BR)	36.26	1,119,184	0.04	20 m grid
5	Caxiuanã (BR)	28.64	229,121	0.04	20 m grid
6	Nouragues (FG)	37.26	422,834	0.04	10 m grid
7	Nouragues (FG)	46.49	919,658	0.04	10 m grid
8	London (UK)	23.37	4,023,751	0.04	Circle around the tree
9	Ankasa Forest Reserve (GH)	34.18	499,890	0.04	10 m grid
10	Ankasa Forest Reserve (GH)	38.41	414,382	0.04	10 m grid

Note. Grid scan pattern means a uniform grid with 10 m or 20 m spacing between consecutive scans.
UK: United Kingdom; BR: Brazil; FG: French Guyana; GH: Ghana.

selected and manually classified as wood or leaf. Separation was then carried out using the algorithm *generic_tree*, presented in Figure 4.

We performed two sets of tests: running once for each tree using default input parameters; and running 10 times for each tree using pseudo-randomly chosen parameters values. In the first set of tests results were recorded at each major step of the separation. For the second group of tests, parameters values were pseudo-randomly selected for each test and each tree. The pool of possible parameter values is shown in Table 5. As the voting separation requires more than one value for number of neighbours (*knn*), and following the default option, five different *knn* values were selected for each test.

2.4.3 | Performance assessment

Three metrics were used to assess the performance of the separation: accuracy, Cohen's κ and *F*-score. These metrics were applied to all tests. All metrics are calculated from elements of confusion matrices (Table 6), which contain correct and incorrect separation results for both classes.

T_w is the number of points correctly classified as wood, F_w the number of points incorrectly classified as wood, T_l the number of points correctly classified as leaf and F_l the number of points incorrectly classified as leaf, that is true/false positive wood and leaf respectively. Accuracy, as used in Tao et al. (2015), is defined by Equation (1):

$$\text{accuracy} = \frac{T_w + T_l}{T_w + F_w + T_l + F_l}. \quad (1)$$

F-score (Equation 4) uses the terms precision (*p*) and recall (*r*) (Equations 2 and 3), based on Sokolova, Japkowicz, and Szpakowicz (2006) but presented as in Tao et al. (2015). However, because *F*-score is based on true positives, this metric was calculated twice to cover both classes.

$$p = \frac{T_w}{T_w + F_w} \times \frac{T_l}{T_l + F_l} \quad (2)$$

$$r = \frac{T_w}{T_w + F_l} \times \frac{T_l}{T_l + F_w} \quad (3)$$

TABLE 5 Set of separation input parameter values used in pseudo-random selection for validation tests

Parameter	Possible values
Number of neighbours (knn)	10, 20, 30, 40, 50, 60, 70, 80, 90, 100, 110, 120, 130, 140, 150, 160, 170, 180, 190, 200, 210, 220, 230, 240, 250
Voxel size (m)	0.03, 0.05, 0.07, 0.09, 0.11, 0.13, 0.15
Steps to retrace	30, 40, 50, 60, 70, 80, 90, 100

$$F = \frac{2 \times r \times p}{r + p} \quad (4)$$

Cohen's κ coefficient (Equation 6) uses proportionate agreement (*po*), which has the same definition as accuracy (Equation 1), and probability of random agreement (*pe*) (Equation 5). The term *N* in Equation (5) represents the sum of all elements in a confusion matrix, that is total number of points.

$$pe = \frac{(T_w + F_l) \times (T_w + F_w)}{N} + \frac{(F_w + T_l) \times (F_l + T_l)}{N} \quad (5)$$

$$k = \frac{po - pe}{1 - pe}. \quad (6)$$

3 | RESULTS

3.1 | Simulated data

Validation metrics using simulated data are presented in Table 7. Average per tree separation accuracy ranged from 0.77 to 0.89. Overall accuracy had an average of 0.83 and standard deviation of 0.06. Figure 6 presents accuracy per tree calculated for all 50 tests. TICO2 and ACPL presented the highest accuracy, 0.89. These trees also had the best results for leaf classification, 0.92 and 0.93, for ACPL and TICO2 respectively. Results from ALGL3 presented the lowest

TABLE 6 Confusion matrix used in pointwise assessment of separation results

	Recognized	
Class	As wood (C_w)	As leaf (C_l)
Wood (W)	T_w	F_l
Leaf (L)	F_w	T_l

overall accuracy and largest variance. *F*-scores for wood points are mostly lower than those for leaf class. The only exception in this case occurred in tests using BEPE2. Kappa presented the same pattern as accuracy, with a clear difference between ACPL/TICO2 and ALGL3/BEPE2. An analysis of all kappa components confirms that separations for ALGL3 and BEPE2, both with lower kappa, had a much higher frequency of false wood points than false leaf points, up to averages of 0.11 and 0.18 for BEPE2 and ALGL3 respectively (Figure 7).

When stacking all resulting wood and leaf clouds for each simulated tree, we see that the majority of points are successfully detected even in cases of lower accuracy, such as for BEPE2 (Figure 8).

Results from simulated clouds were also superficially assessed in terms of point cloud quality. Figure 9 shows that even for low-quality clouds (i.e. average distance between neighbouring points of 5.6 cm) the algorithm still produced results with accuracy above 0.8. Visually, the same pattern as Figure 8 is seen in Figure 9, in which larger wood structures were successfully separated and most false positives happen in points from smaller branches and leaves.

3.2 | Field data

Metrics for the TLS data are similar to results from simulated data (Table 8), albeit with higher variability. In general, accuracies from field data are higher than for simulated, with averages of 0.89 and 0.83 respectively. Results in Figure 10 also demonstrate that most of the wood structure is also detected correctly.

Average accuracy from intermediary steps is above 0.74. Steps based on absolute threshold separation obtained the worst overall results. Path retrace and reference voting separation generated clouds with highest average accuracy, but differed slightly in regards to success in wood detection. The step-by-step analysis (Table 9) accentuated the diverging pattern in *F*-scores already seen in Tables 7 and 8, with wood detection presenting much lower scores.

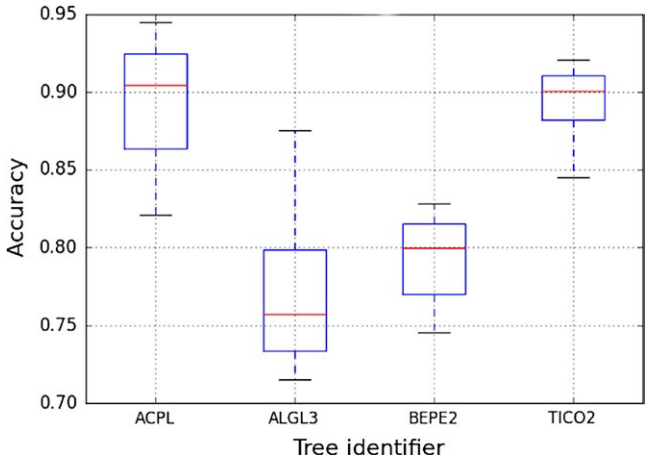

FIGURE 6 Box whisker showing separation accuracy for simulated trees (50 tests for each tree). The box dimensions show the quartiles for 25%–75% of accuracy, the red line represents median accuracy and the whiskers show minimum and maximum accuracy

Figure 11 shows accuracy from tests using pseudo-randomly selected parameters. In most cases, average accuracy of each tree was close to results using default parameters (red marker). Tree_13 presented highest overall accuracy and was the only tree with all values from the pseudo-random test better than default parameters. The largest accuracy variation, with a range of 0.13, was obtained for alice_2, which was also the only tree with the most accurate results when using default parameters.

4 | DISCUSSION

We validated the separation in two distinct ways: (a) using a generic testing framework with simulated TLS data, (b) using measured TLS data, where accuracy is assessed through random sampling and manual classification of points. The use of simulated data (a) overcomes limitations of field data (b) where a fiduciary or reference truth is not known a priori.

4.1 | Simulated data

We tested our algorithm on 200 point clouds generated through random combinations of TLS simulations from four tree models (Table 3). Accuracies shown in Table 7 are comparable to results

TABLE 7 Overall mean and standard deviation (*SD*) for each tree from validation using simulated data

	Accuracy		*F*-wood		*F*-leaf		κ	
Tree name	*M*	*SD*	*M*	*SD*	*M*	*SD*	*M*	*SD*
ACPL	0.89	0.03	0.84	0.07	0.92	0.02	0.76	0.09
ALGL3	0.77	0.04	0.70	0.03	0.81	0.05	0.52	0.06
BEPE2	0.79	0.03	0.81	0.03	0.76	0.03	0.57	0.05
TICO2	0.89	0.02	0.79	0.05	0.93	0.01	0.72	0.05

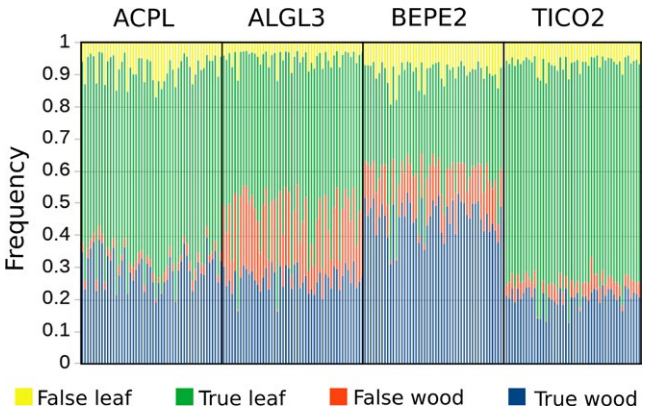

FIGURE 7 Components of confusion matrix used to calculate kappa for each test using simulated cloud (50 tests for each tree)

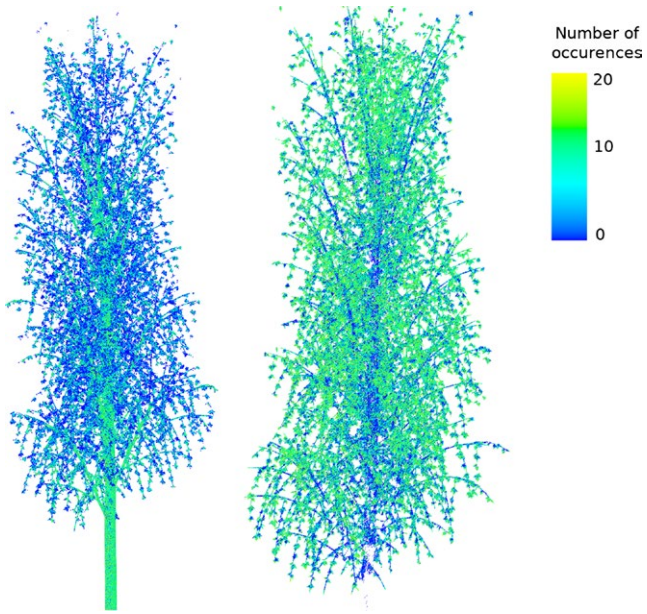

FIGURE 8 Total number of points accumulated for all 50 simulated BEPE2 clouds used in the validation dataset

in the literature of separation for simulated data (Tao et al., 2015).

F-scores suggest that, in three of the four cases, an accurate wood classification is harder to achieve than for leaf material. Also, lower kappa indicates that misclassification in both classes affects separation accuracy. Visual inspection of results (Figures 8 and 9) shows that most of the wood structure was successfully classified, despite wood points showing lower *F*-scores. Kappa components (Figure 7) shows similar results of misclassified leaf (false leaf) points across all trees, but a much higher rate of false wood points for trees with lower accuracy/kappa. Comparison between individual leaf area (Table 3) and false wood counts (Figure 7) suggests that smaller leaves might impact the resulting arrangement of points making them more difficult to be separated. In the case of our simulated dataset, both trees with smaller leaves were also the tallest, which might have increased the difficulty to separate wood and leaf points even further due to larger laser footprints. Different neighbourhood sizes should be studied as a potential adjustment to overcome such difficulties. This is something that is difficult to do with real data, and so may be more practical using the simulated point cloud approach we use above.

Figure 9 suggests that although point density can also be an obstacle to leaf-wood separation, our method is robust enough to overcome it in many cases.

Results from simulated datasets demonstrate the potential of using our separation algorithm. Further per-tree parameter optimization still needs to be assessed more fully but can potentially improve results. A thorough parameter selection can be performed using a testing framework, such as LiDARtf. Using simulated data as we have done here has the considerable advantage of being entirely reproducible and provides the means to further optimize processing and allow comparison between different leaf-wood separation methods.

4.2 | Field data

We tested our separation algorithm on 10 point clouds from real trees, scanned in several locations in different continents and forest types. Accuracies for separation using default parameters are within 10% to those presented by Ma et al. (2016) and Zhu et al. (2018), albeit operating in a completely automated setting.

Similar to results from simulated data, around 90% of the wood structure was detected correctly (Figure 10). However, the slightly poorer scan quality in field conditions might have increased the divergence between leaf and wood point arrangements, helping to reduce the occurrence of false positives and negatives. The best performance using default parameters values was obtained with a tropical tree (nouraguesH20_10), which are usually difficult to scan in high quality due to occlusion and canopy heights.

Results from intermediary steps show that path detection and geometric feature classification using a voting scheme obtained the highest average accuracy. Although such results might suggest that a simplification of our algorithm is possible by removing absolute threshold separation, such approach has shown to be capable of detecting smaller branches (see, e.g. Supporting Information). In this sense, absolute threshold classifications are used to add redundancy to our automated separation algorithm. Positive results from path detection approaches (Table 9 and Figures 2 and 3) indicates that their inclusion is valuable to ensure robustness over different tree types and scan quality. Therefore, we suggest that the algorithm presented in this paper is suitable as it is and recommended for automated leaf/wood separation of single tree point clouds.

Tests using pseudo-randomly selected parameters indicates that although default parameters are capable of obtaining results with accuracy above 0.8, a per tree parameter optimization can achieve higher accuracy. This suggests that it is possible to process the same tree using a range of values for each parameter in order to obtain the best results. Also, as suggested by results shown in Figure 8, processing the same tree several times and accumulating the resulting points is another way of using a voting scheme that might yield separated clouds with even higher accuracy.

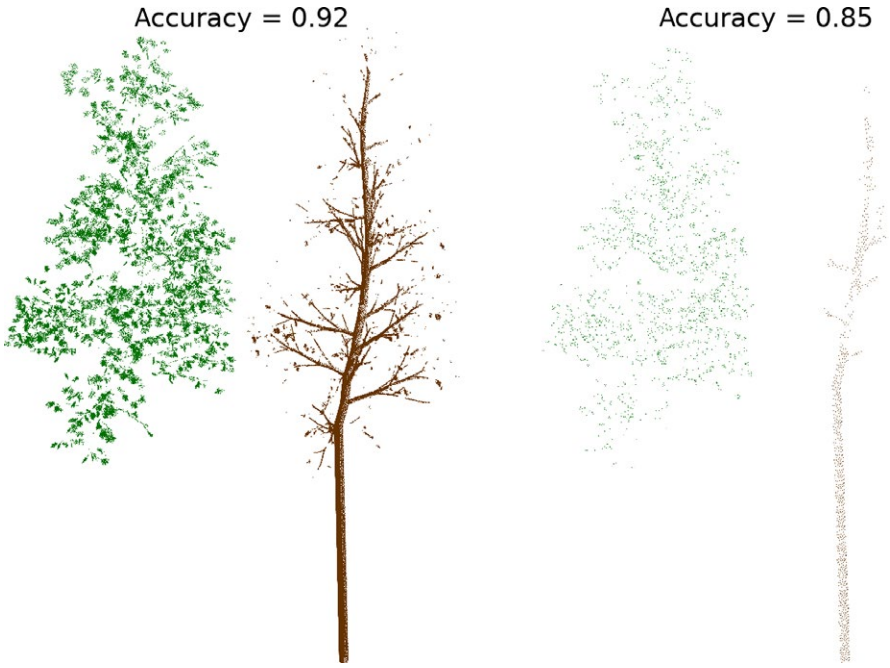

FIGURE 9 Point density impact on separation accuracy from two sets of ACPL simulated point clouds. Left: results from high point density (average distance between neighbouring points of 1.2 cm); Right: results from low point density (average distance between neighbouring points of 5.6 cm)

TABLE 8 Validation summary for Terrestrial Laser Scanning field data

Tree index	Tree name	Accuracy	*F*-score wood	*F*-score leaf	κ
1	alice 1	0.90	0.74	0.94	0.68
2	alice 2	0.90	0.69	0.94	0.63
3	alice 3	0.86	0.69	0.90	0.60
4	caxiuanaA117	0.89	0.67	0.93	0.60
5	caxiuanaA21	0.85	0.64	0.91	0.55
6	nouraguesH20 108	0.93	0.82	0.95	0.77
7	nouraguesH20 13	0.89	0.69	0.93	0.63
8	pan 33	0.88	0.58	0.89	0.48
9	tree 13	0.90	0.86	0.92	0.78
10	tree 2	0.91	0.89	0.92	0.81

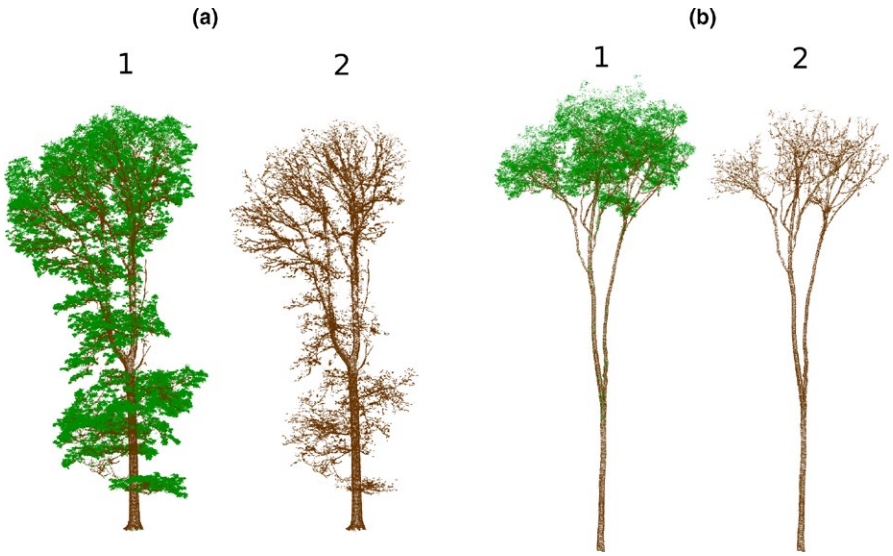

FIGURE 10 Example of separated point clouds of a tree from temperate forest (a – Alice Holt, UK) and tropical forest (b – Nouragues, FG). a1 and b1 represent the coloured results of the separation, in which wood points are shown in brown and leaf points in green. a2 and b2 represent only the separated wood points

TABLE 9 Validation summary for each step of the automated separation using Terrestrial Laser Scanning field data

Step	Accuracy	*F*-wood	*F*-leaf	κ
Path frequency	0.84	0.51	0.90	0.43
Path retrace	0.89	0.62	0.93	0.56
Threshold Separation 1	0.75	0.31	0.84	0.22
Reference vote separation	0.89	0.68	0.93	0.62
Threshold Separation 2	0.77	0.23	0.86	0.14
Threshold Separation 3	0.74	0.12	0.84	0.06
Final separation	0.88	0.69	0.92	0.61

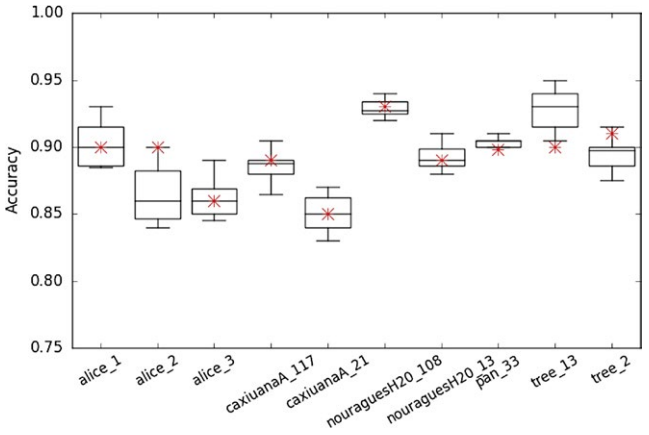

FIGURE 11 Box whisker showing accuracy for tests using pseudo-randomly selected parameters from Table 5 applied to measured Terrestrial Laser Scanning field data. Red markers represent accuracy obtained using default input parameters. The box dimensions show the quartiles for 25%–75% of accuracy, the centre horizontal line represents median accuracy and the whiskers show minimum and maximum accuracy values

Results show that our algorithm can separate field data with accuracy above 90%, even in less than optimal circumstances and without requiring any manual intervention or prior knowledge about the dataset. Even in cases with lower accuracy, separation results should not have negative impact on further processing as more than 85% of wood and leaf structure was successfully classified. Separation of wood and leaf in TLS point clouds is a key step in the estimation of either wood or leaf properties alone. Here, we provide tools that will hopefully enable other researchers to address this aspect.

Validation using simulated data suggests that data quality has an impact in the separation accuracy and this effect is also true for field data. Some important sources of uncertainty related to data quality, such as co-registration accuracy and occlusion levels, were not addressed in this paper. So far, to the best of our knowledge, there is no tool available for simulating co-registration accuracy and occlusion and it is very difficult to precisely quantify them on a tree level basis from field data. Some scanners characteristics such as beam divergence, ranging accuracy, spectral sensitivity, wavelength decomposition and angular step resolution also play a role in point cloud quality. Although validation data were obtained using a RIEGL VZ-400 (and simulating this instrument's characteristics), our method does not depend on a specific scanner and we expect similar results from other instruments with similar capabilities. Results presented in this paper suggest that the redundancy present in our automated method is capable to separate leaf and wood materials, as long as point clouds present a reasonable quality (e.g. no large portions occluded, point density large enough to resolve different structures and sub centimetre co-registration accuracy). Therefore, for best results we suggest the use of high resolution TLS instruments and the application of optimal field scanning protocols and co-registration methodology such as presented in Wilkes et al. (2017).

Processing times recorded while separating field data showed that it takes around 60 s for every 100,000 points to run a single tree point cloud (recorded timings in Supporting Information). Also, recorded times indicate that processing time scales linearly with number of points.

4.3 | Separation library

Results presented here demonstrate the possible applications of our automated separation algorithm, available in the TLSeparation library. Further studies are suggested to better understand how point cloud quality relates to separation accuracy. Testing a range of parameters over the same dataset has shown potential in improving accuracy with per tree parameter optimization. Further tests should also give insight into how to best automate the optimization of a set of parameters. This approach requires a consistent analysis and a standardized testing framework, such as LiDARtf. Our framework is, so far and to the best of our knowledge, the only approach to validate a separation method completely and without user classification bias, or to compare between different methods.

The library presented here is open-source and available to be installed and used out-of-the-box. Our library is hosted by Python Package Index and its installation process is automated. Such ease of use should improve further processing of larger numbers of TLS datasets for a larger audience. All tests presented here are from a single automated algorithm, however, the possibility of easily adapting or creating new algorithms should also be useful when high levels of accuracy are required for a particular dataset.

Although only the separation of point clouds from individual broadleaf trees was addressed in this paper, most of the tools already implemented in this library are applicable to plot-wide data and needleleaf trees. For example a plot-wide separation could use the same algorithm presented here for individual trees (*generic_tree*) without steps based on path classification. Given the differences of leaf and needle point arrangement, needleleaf trees were not included in this study as they require a change in scanning protocol (to better resolve needles) or separation approach. Preliminary tests suggest that it is possible to separate materials from needleleaf trees

using the methods in TLSeparation, but it would require a different automated workflow to achieve similar accuracies as the ones showed in this paper. New algorithms specifically aimed for needle-leaf trees and plot-wide data are under development and will be added to TLSeparation in future update cycles.

TLSeparation was developed as a base library to support development and extension of TLS separation methodologies. It is our hope that the TLS/ecology community can take advantage of this library to create workflows that are optimized for specific use cases and then share it with other potential users. Along with a standard testing framework, such as LiDARtf, this library should help to improve material separation and the understanding about its impacts on TLS estimates of canopy properties.

5 | CONCLUSIONS

In this study, we demonstrate the use of an open-source automated separation procedure to classify leaf and wood materials from point clouds of individual trees. Results from our method were similar to other results found in the literature. This is not surprising in that our approach builds on and extends previous work. The major difference is that our approach is completely automated, unlike other methods. This makes it potentially more suitable for applications involving more than a few trees. Direct comparison of different methods has been impractical or even impossible previously due to lack of standardized datasets with reference values. We present a testing framework designed for a complete and reproducible validation. Inclusion of a path detection approach to better separate materials in lower quality data is shown to be an improvement over previous approaches. Similar accuracy values are obtained across validation examples using quite different measured TLS configurations and tree types. This suggests that our combination of different approaches is robust and transferable without requiring any changes to our algorithm or user input. Impact of leaf and wood separation on subsequent TLS methods is still unknown and we recommend future studies to address this important aspect of TLS estimates. The automated script is part of a leaf/wood separation software package, which can be easily modified and/or extended to fit specific requirements. The use of this library by the scientific community could generate better, more specific, separation workflows and adequate means to compare and validate them.

ACKNOWLEDGEMENTS

M.B.V. is funded by CNPq (National Council of Technological and Scientific Development – Brazil) through the programme Science Without Borders (Process number 233849/2014-9). M.D. an P.W. acknowledge NERC NCEO support for travel and capital funding for LiDAR equipment. M.D. was supported in part by NERC Standard Grants NE/N00373X/1 and NE/P011780/1, CNRS Nouragues Travel Grants Program, ESA BIOMASS calibration/validation funding and the European Union's Horizon 2020 research and innovation programme under grant agreement No 640176 for the EU H2020 BACI project. K.C. is funded by BELSPO (Belgian Science Policy Office) in the frame of the STEREO III programme – project 3D-FOREST (SR/02/355). We gratefully acknowledge the assistance of the following people for site access and field support: Eric Casella, Forest Research (Alice Holt – UK); Lucy Rowland, Lola da Costa, Ed Mitchard and Patrick Meir (Caxiuanã BR); Jerome Chave and Blaise Tymen (Nouragues – FG); Justice Mensah (Ankasa – GH). We also thank the anonymous reviewers for their constructive comments .

AUTHORS' CONTRIBUTIONS

M.B.V. led the entire study and developed the separation methodology; M.B.V., M.D. and W.W. conceived the TLS data simulation; M.B.V., M.D., P.W., K.C. and A.B. collected field data; All authors contributed critically to validation design, drafts and gave final approval for publication.

DATA ACCESSIBILITY

The testing framework used in our validation, LiDARtf, is Open Source under license GPL-3.0 and hosted at https://zenodo.org/record/802379#.WzVrmBzTVqM. More information and instructions on how to install and use the TLSeparation library can be found at https://tlseparation.github.io/documentation/index.html. The source code for TLSeparation is OpenSource under GPL-3.0 license and hosted at https://zenodo.org/record/1147706#.WzVrkxzTVqM. Field and simulated datasets used in the validation are, respectively, hosted at https://doi.org/10.5281/zenodo.1324155 and https://doi.org/10.5281/zenodo.1324157.

ORCID

Matheus B. Vicari https://orcid.org/0000-0001-8841-4205
Mathias Disney https://orcid.org/0000-0002-2407-4026
Andrew Burt https://orcid.org/0000-0002-4209-8101

REFERENCES

Béland, M., Baldocchi, D. D., Widlowski, J. L., Fournier, R. A., & Verstraete, M. M. (2014). On seeing the wood from the leaves and the role of voxel size in determining leaf area distribution of forests with terrestrial LiDAR. *Agricultural and Forest Meteorology*, *184*, 82–97. https://doi.org/10.1016/j.agrformet.2013.09.005

Béland, M., Widlowski, J. L., Fournier, R. A., Côté, J. F., & Verstraete, M. M. (2011). Estimating leaf area distribution in savanna trees from terrestrial LiDAR measurements. *Agricultural and Forest Meteorology*, *151*, 1252–1266. https://doi.org/10.1016/j.agrformet.2011.05.004

Calders, K., Disney, M. I., Armston, J., Burt, A., Brede, B., Origo, N., … Nightingale, J. (2017). Evaluation of the range accuracy and the radiometric calibration of multiple terrestrial laser scanning instruments for data interoperability. *IEEE Transactions on Geoscience and Remote Sensing*, *55*, 2716–2724. https://doi.org/10.1109/TGRS.2017.2652721

Calders, K., Newnham, G., Burt, A., Murphy, S., Raumonen, P., Herold, M., … Kaasalainen, M. (2015). Nondestructive estimates of above-ground biomass using terrestrial laser scanning. *Methods in Ecology and Evolution*, *6*, 198–208. https://doi.org/10.1111/2041-210X.12301

Chen, J. M. (1996). Optically-based methods for measuring seasonal variation of leaf area index in boreal conifer stands. *Agricultural and Forest Meteorology*, *80*, 135–163. https://doi.org/10.1016/0168-1923(95)02291-0

Côté, J. F., Fournier, R. A., Frazer, G. W., & Olaf Niemann, K. (2012). A finescale architectural model of trees to enhance LiDAR-derived measurements of forest canopy structure. *Agricultural and Forest Meteorology*, *166–167*, 72–85.

Côté, J. F., Widlowski, J. L., Fournier, R. A., & Verstraete, M. M. (2009). The structural and radiative consistency of three-dimensional tree reconstructions from terrestrial lidar. *Remote Sensing of Environment*, *113*, 1067–1081.

Cuni-Sanchez, A., White, L. J. T., Calders, K., Jeffery, K. J., Abernethy, K., Burt, A., … Lewis, S. L. (2016). African savanna-forest boundary dynamics: A 20-year study. *PLoS ONE*, *11*, e0156934. https://doi.org/10.1371/journal.pone.0156934

Danson, F. M., Gaulton, R., Armitage, R. P., Disney, M., Gunawan, O., Lewis, P., … Ramirez, A. F. (2014). Developing a dual-wavelength fullwaveform terrestrial laser scanner to characterize forest canopy structure. *Agricultural and Forest Meteorology*, *198–199*, 7–14. https://doi.org/10.1016/j.agrformet.2014.07.007

Danson, F. M., Sasse, F., & Schofield, L. A. (2018). Spectral and spatial information from a novel dual-wavelength full-waveform terrestrial laser scanner for forest ecology. *Interface Focus*, *8*, 20170049. https://doi.org/10.1098/rsfs.2017.0049

Disney, M. I., Boni Vicari, M., Burt, A., Calders, K., Lewis, S. L., Raumonen, P., & Wilkes, P. (2018). Weighing trees with lasers: Advances, challenges and opportunities. *Interface Focus*, *8*, 20170048. https://doi.org/10.1098/rsfs.2017.0048

Disney, M., Lewis, P., & Saich, P. (2006). 3D modelling of forest canopy structure for remote sensing simulations in the optical and microwave domains. *Remote Sensing of Environment*, *100*, 114–132. https://doi.org/10.1016/j.rse.2005.10.003

Do, C. B., & Batzoglou, S. (2008). What is the expectation maximization algorithm? *Nature Biotechnology*, *26*, 897–899. https://doi.org/10.1038/nbt1406

Douglas, E. S., Martel, J., Li, Z., Howe, G., Hewawasam, K., Marshall, R. A., … Chakrabarti, S. (2015). Finding leaves in the forest: The dual-wavelength Echidna lidar. *IEEE Geoscience and Remote Sensing Letters*, *12*, 776–780. https://doi.org/10.1109/LGRS.2014.2361812

Douglas, E. S., Strahler, A., Martel, J., Cook, T., Mendillo, C., Marshall, R., … Lovell, J. (2012) *DWEL: A Dual-Wavelength Echidna Lidar for ground-based forest scanning*. International Geoscience and Remote Sensing Symposium (IGARSS) (pp. 4998–5001).

Ester, M., Kriegel, H. P., Sander, J., & Xu, X. (1996) A density-based algorithm for discovering clusters a density-based algorithm for discovering clusters in large spatial databases with noise. *Proceedings of the second international conference on knowledge discovery and data mining*, *KDD'96* (pp. 226–231). Menlo Park, CA: AAAI Press.

Gonzalez de Tanago, J., Lau, A., Bartholomeus, H., Herold, M., Avitabile, V., Raumonen, P., … Calders, K. (2018). Estimation of above-ground biomass of large tropical trees with terrestrial LiDAR. *Methods in Ecology and Evolution*, *9*, 223–234. https://doi.org/10.1111/2041-210X.12904

Grau, E., Durrieu, S., Fournier, R., Gastellu-Etchegorry, J. P., & Yin, T. (2017). Estimation of 3D vegetation density with Terrestrial Laser Scanning data using voxels. A sensitivity analysis of influencing parameters. *Remote Sensing of Environment*, *191*, 373–388. https://doi.org/10.1016/j.rse.2017.01.032

Hancock, S., Gaulton, R., & Danson, F. M. (2017). Angular reflectance of leaves with a dual-wavelength terrestrial lidar and its implications for leaf-bark separation and leaf moisture estimation. *IEEE Transactions on Geoscience and Remote Sensing*, *55*, 3084–3090. https://doi.org/10.1109/TGRS.2017.2652140

Hosoi, F., Nakai, Y., & Omasa, K. (2013). 3-D voxel-based solid modeling of a broad-leaved tree for accurate volume estimation using portable scanning lidar. *ISPRS Journal of Photogrammetry and Remote Sensing*, *82*, 41–48. https://doi.org/10.1016/j.isprsjprs.2013.04.011

Jupp, D. L. B., & Lovell, J. L. (2007). *Airborne and ground-based lidar systems for forest measurement: Background and principles*. Canberra, ACT: CSIRO Marine and Atmospheric Research.

Lewis, P. (1999). Three-dimensional plant modelling for remote sensing simulation studies using the Botanical Plant Modelling System. *Agronomie*, *19*, 185–210. https://doi.org/10.1051/agro:19990302

Li, Z., Schaefer, M., Strahler, A., Schaaf, C., & Jupp, D. (2018). On the utilization of novel spectral laser scanning for three-dimensional classification of vegetation elements. *Interface Focus*, *8*, 20170039. https://doi.org/10.1098/rsfs.2017.0039

Li, Z., Strahler, A., Schaaf, C., Jupp, D., Schaefer, M., & Olofsson, P. (2018). Seasonal change of leaf and woody area profiles in a midlatitude deciduous forest canopy from classified dual-wavelength terrestrial lidar point clouds. *Agricultural and Forest Meteorology*, *262*, 279–297. https://doi.org/10.1016/j.agrformet.2018.07.014

Liang, X., Kankare, V., Hyyppä, J., Wang, Y., Kukko, A., Haggrén, H., … Vastaranta, M. (2016). Terrestrial laser scanning in forest inventories. *ISPRS Journal of Photogrammetry and Remote Sensing*, *115*, 63–77. https://doi.org/10.1016/j.isprsjprs.2016.01.006

Ma, L., Zheng, G., Eitel, J. U. H., Moskal, L. M., He, W., & Huang, H. (2016). Improved salient feature-based approach for automatically separating photosynthetic and nonphotosynthetic components within terrestrial lidar point cloud data of forest canopies. *IEEE Transactions on Geoscience and Remote Sensing*, *54*, 679–696. https://doi.org/10.1109/TGRS.2015.2459716

Malhi, Y., Jackson, T., Patrick Bentley, L., Lau, A., Shenkin, A., Herold, M., … Disney, M. I. (2018). New perspectives on the ecology of tree structure and tree communities through terrestrial laser scanning. *Interface Focus*, *8*, 20170052. https://doi.org/10.1098/rsfs.2017.0052

Momo Takoudjou, S., Ploton, P., Sonké, B., Hackenberg, J., Griffon, S., de Coligny, F., … Barbier, N. (2018). Using terrestrial laser scanning data to estimate large tropical trees biomass and calibrate allometric models: A comparison with traditional destructive approach. *Methods in Ecology and Evolution*, *9*, 905–916. https://doi.org/10.1111/2041-210X.12933

Nevalainen, O., Hakala, T., Suomalainen, J., Mäkipää, R., Peltoniemi, M., Krooks, A., & Kaasalainen, S. (2014). Fast and nondestructive method for leaf level chlorophyll estimation using hyperspectral LiDAR. *Agricultural and Forest Meteorology*, *198*, 250–258. https://doi.org/10.1016/j.agrformet.2014.08.018

Raumonen, P., Kaasalainen, M., Åkerblom, M., Kaasalainen, S., Kaartinen, H., Vastaranta, M., … Lewis, P. (2013). Fast automatic precision tree models from terrestrial laser scanner data. *Remote Sensing*, *5*, 491–520. https://doi.org/10.3390/rs5020491

Sokolova, M., Japkowicz, N., & Szpakowicz, S. (2006). Beyond accuracy, FScore and ROC: A family of discriminant measures for performance evaluation. *Advances in Artificial Intelligence*, *4304*, 1015–1021.

Strahler, A. H., Jupp, D. L., Woodcock, C. E., Schaaf, C. B., Yao, T., Zhao, F., … Boykin-Morris, W. (2008). Retrieval of forest structural parameters using a ground-based lidar instrument (Echidna®). *Canadian Journal of Remote Sensing*, *34*, S426–S440. https://doi.org/10.5589/m08-046

Tao, S., Guo, Q., Xu, S., Su, Y., Li, Y., & Wu, F. (2015). A geometric method for wood-leaf separation using terrestrial and simulated lidar data. *Photogrammetric Engineering & Remote Sensing*, *81*, 767–776. https://doi.org/10.14358/PERS.81.10.767

Vicari, M. B. (2017a) *LiDARTF—A testing framework for LiDAR data processing*. https://doi.org/10.5281/zenodo.802378

Vicari, M. B. (2017b) *TLSeparation—A Python library for material separation from tree/forest 3D point clouds*. https://doi.org/10.5281/zenodo.1147705

Wang, Z., Zhang, L., Fang, T., Mathiopoulos, P. T., Tong, X., Qu, H., … Chen, D. (2015). A multiscale and hierarchical feature extraction method for terrestrial laser scanning point cloud classification. *IEEE Transactions on Geoscience and Remote Sensing*, *53*, 2409–2425. https://doi.org/10.1109/TGRS.2014.2359951

Widlowski, J. L., Mio, C., Disney, M., Adams, J., Andredakis, I., Atzberger, C., … Zenone, T. (2015). The fourth phase of the radiative transfer model intercomparison (RAMI) exercise: Actual canopy scenarios and conformity testing. *Remote Sensing of Environment*, *169*, 418–437. https://doi.org/10.1016/j.rse.2015.08.016

Wilkes, P., Lau, A., Disney, M., Calders, K., Burt, A., Gonzalez de Tanago, J., … Herold, M. (2017). Data acquisition considerations for terrestrial laser scanning of forest plots. *Remote Sensing of Environment*, *196*, 140–153. https://doi.org/10.1016/j.rse.2017.04.030

Woodgate, W., Armston, J. D., Disney, M., Jones, S. D., Suarez, L., Hill, M. J., … Soto-Berelov, M. (2016). Quantifying the impact of woody material on leaf area index estimation from hemispherical photography using 3D canopy simulations. *Agricultural and Forest Meteorology*, *226227*, 1–12. https://doi.org/10.1016/j.agrformet.2016.05.009

Zhao, K., García, M., Liu, S., Guo, Q., Chen, G., Zhang, X., … Meng, X. (2015). errestrial lidar remote sensing of forests: Maximum likelihood estimates of canopy profile, leaf area index, and leaf angle distribution. *Agricultural and Forest Meteorology*, *209–210*, 100–113. https://doi.org/10.1016/j.agrformet.2015.03.008

Zhu, X., Skidmore, A. K., Darvishzadeh, R., Niemann, K. O., Liu, J., Shi, Y., & Wang, T. (2018). Foliar and woody materials discriminated using terrestrial LiDAR in a mixed natural forest. *International Journal of Applied Earth Observation and Geoinformation*, *64*, 43–50.

SUPPORTING INFORMATION

Additional supporting information may be found online in the Supporting Information section at the end of the article.

How to cite this article: Vicari MB, Disney M, Wilkes P, Burt A, Calders K, Woodgate W. Leaf and wood classification framework for terrestrial LiDAR point clouds. *Methods Ecol Evol*. 2019;10:680–694. https://doi.org/10.1111/2041-210X.13144